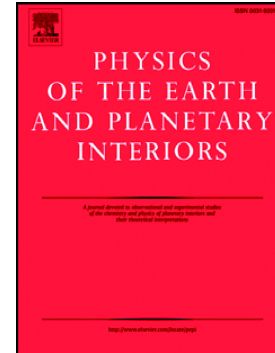


Journal Pre-proof

New high precision full-vector archaeomagnetic data from a roman kiln in MÉRIDA (Spain)

N. García-Redondo, M. Calvo-Rathert, A. Carrancho, M. Bustamante-Álvarez



PII: S0031-9201(20)30081-9

DOI: <https://doi.org/10.1016/j.pepi.2020.106591>

Reference: PEPI 106591

To appear in: *Physics of the Earth and Planetary Interiors*

Received date: 19 March 2020

Revised date: 19 July 2020

Accepted date: 22 September 2020

Please cite this article as: N. García-Redondo, M. Calvo-Rathert, A. Carrancho, et al., New high precision full-vector archaeomagnetic data from a roman kiln in MÉRIDA (Spain), *Physics of the Earth and Planetary Interiors* (2020), <https://doi.org/10.1016/j.pepi.2020.106591>

This is a PDF file of an article that has undergone enhancements after acceptance, such as the addition of a cover page and metadata, and formatting for readability, but it is not yet the definitive version of record. This version will undergo additional copyediting, typesetting and review before it is published in its final form, but we are providing this version to give early visibility of the article. Please note that, during the production process, errors may be discovered which could affect the content, and all legal disclaimers that apply to the journal pertain.

© 2020 Published by Elsevier.

NEW HIGH PRECISION FULL-VECTOR ARCHAEO-MAGNETIC DATA FROM A ROMAN KILN IN MÉRIDA (SPAIN)

N. García-Redondo¹, M. Calvo-Rathert^{1,2}, A. Carrancho³, M. Bustamante-Álvarez⁴

¹Laboratorio de Paleomagnetismo, Dpto. Física, Avda Cantabria s/n, Universidad de Burgos, 09006 Burgos, Spain. ngredondo@ubu.es ; mcalvo@ubu.es

²Hawaii Institute of Geophysics and Planetology – University of Hawaii at Manoa, 1680 East-West Rd., 96822 Honolulu, HI, United States.

³Área de Prehistoria, Departamento de Historia, Geografía y Comunicación, Universidad de Burgos, Edificio I+D+I, Plaza Misael Dañuelos s/n, 09001 Burgos, Spain. acarrancho@ubu.es

⁴Área de Arqueología, Departamento de Prehistoria y Arqueología, Facultad de Filosofía y Letras. Campus Cartuja s/n, 18071, Granada, Spain. mbustamante@ugr.es

*Corresponding author: Tel.: +34 917 258 978 *Email address:* ngredondo@ubu.es (Natalia García-Redondo)

ABSTRACT

This study presents new high precision age and full-vector archaeomagnetic data from a kiln excavated in the Roman archaeological site of Mitreo's house (Mérida, Badajoz, Spain). The age of the kiln was obtained by the stratigraphic method and by the ceramological study of the *italic* and *sigillata* pottery found with a very precise age date of 55 ± 15 years AD. Rock-magnetic experiments pointed towards magnetite as the main carrier of remanence and highly reversible thermomagnetic curves suggested that the studied samples were suitable for archaeointensity determinations. Paleomagnetic experiments including thermal and stepwise alternating field demagnetization yielded the following mean direction for the kiln: declination $D = 0.6^\circ$; inclination $I = 54.0^\circ$; (k

= 481; $\alpha_{95} = 2.5^\circ$). Archaeointensity experiments with the Thellier – Coe protocol on 28 samples yielded successful determinations in 27 cases. Anisotropy factors between 0.90 and 1.04 were obtained from anisotropy of thermoremanent magnetization (ATRM) experiments. A mean anisotropy-corrected archaeointensity value $F = 56.3 \pm 5.5 \mu\text{T}$ was obtained.

The geomagnetic model SHA.DIF.14k was used for an archaeomagnetic dating yielding a chronological interval between 40 BCE and 150 AD. This low age resolution when compared with the pottery-based age data is related to the behavior of the geomagnetic field in the Iberian Peninsula during the Roman period which does not allow to differentiate well between results corresponding to those centuries. However, it is also related to the fact that the Iberian archaeomagnetic dataset in the analyzed time range is highly scattered. A high quality full-vector data with a very precise age have been obtained which contribute to improve the Iberian secular variation curve and geomagnetic databases.

KEY WORDS

Archaeomagnetism, Archaeointensity, Paleoeccular Variation Curve, Magnetic properties, Roman period, Iberian Peninsula

1. INTRODUCTION

The archaeomagnetic dating technique, is based on the knowledge of the directional and/or intensity variations of the Earth's magnetic field (EMF) with time, and it is a valuable tool increasingly used to date archaeological combustion structures for the last millennia (e.g.: Ruiz-Martinez et al., 2008; Casas et al., 2018; Carrancho et al., 2017). In addition, information about temporal variations of the EMF is necessary to understand and model the characteristics of the field.

The archaeomagnetic technique is based on the ability of burnt archaeological materials (e.g.: kilns, potteries, bricks, etc) to register the direction and/or the intensity of the EMF when, after being heated above its Curie temperature, the archaeological material cools down in the presence of the EMF to room temperature, acquiring a thermal remanent magnetization (TRM). One of the advantages of archaeomagnetic dating (e.g., García-Redondo et al., 2020; Casas et al. 2018) on materials carrying a TRM signal is that this technique dates the precise time of the last heating to which the analyzed material has been subjected. The last heating of an archaeological combustion structure is usually associated with the end of its use or the abandonment of the site (e.g., García-Redondo et al., 2019; Casas et al., 2018). By comparing the mean direction and archaeointensity values of the samples with a geomagnetic field model or an available regional secular variation curve the age of the magnetization (its last use) can be determined. This yields valuable information in comparison with other dating techniques such as radiocarbon, whose age is determined on samples that may have been burnt multiple times but the dating does not necessarily correspond to the last one. Another advantage is that radiocarbon, a widely used dating technique in archaeology, has a plateau between 800 and 400 BCE (the Hallstattian plateau), not allowing to date with ^{14}C with a precision lower than ~ 400 years (Hervé and Lanos, 2018). Moreover, in archaeological combustion structures used multiple times such as pottery kilns or domestic ovens, it is likely that the magnetization is recorded through a full TRM. This ensures a reliable and instantaneous magnetic record at the time of last burning and subsequent cooling.

The EMF variation pattern changes at a global and regional scale. Paleosecular variation curves (PSVc) and regional geomagnetic field models (e.g.: Pavón-Carrasco et al. 2009) provide information about how the Earth's magnetic field changes at a regional scale

during specific periods of time. Current archaeomagnetic databases are now available covering the last 2-3 millennia for several European regions like, for example the Iberian peninsula (Molina-Cardín et al, 2018; Gómez-Paccard et al, 2006), Germany (Schnepp and Lanos, 2005; Schnepp et al, 2020), France (Gallet et al. 2002 ; Hervè et al. 2013), Greece (De Marco et al., 2008) or Austria (Schnepp and Lanos., 2004), among others. However, records covering longer periods are also available in other parts of Europe or elsewhere (e.g.: Cai et al. 2016; Carrancho et al. 2013; Kovacheva et al. 2014; Tema et al. 2013; Tema and Kondopoulou 2011).

Specific regional geomagnetic field models have been developed from archaeomagnetic and archeointensity data obtained from archaeological burnt materials and lavas (e.g: Pavón-Carrasco et al., 2010; Pavón-Carrasco et al., 2014). This type of models allows determining a secular variation curve avoiding the relocation error. Following the tendency of the EMF, the maximum errors due to the relocation have increased during the last 400 years (Casas and Incoronato, 2007). For Europe they amount to around $0.25^\circ/100\text{km}$ and $100\text{-}200\text{ nT}/100\text{ km}$. (Casas and Incoronato 2007). In this way, it is currently possible to apply archaeomagnetic dating for the last 2-3 millennia (e.g. Palencia-Ortas et al., 2017; Ruiz-Martínez et al., 2008), although the resolution, which oscillates from decades to centuries (e.g.: Casas and Tema, 2019) can vary between different chronologies due to the various factors such as the amount and quality of data, the specific changes that the Earth's magnetic field undergoes at a regional scale.

However, the data from the Iberian PSVc for the Roman period (*ca.* 200 yr BCE – 200 yr AD) present some limitations for archaeomagnetic dating. Firstly, during the Roman period the declination has a low variation in the region. Secondly, the inclination values for the 1st and 2nd centuries AD are very similar to the inclination values observed between the 3rd and the 5th centuries AD. These problems make it difficult to

differentiate between the directional results obtained from certain time intervals during the Roman period (Gómez-Paccard et al., 2013). Although a relatively large amount of data is already available, the uncertainty on direction, intensity and ages is rather high (see Geomagia 50.v3.3, Brown et al., 2015).

Therefore, to increase the accuracy of archaeomagnetic dating in the Roman period a full-vector of the geomagnetic field (declination, inclinations and intensity) is needed to differentiate results from the aforementioned centuries.

Despite their importance, there are still few reliable archaeointensity data in the Iberian Peninsula. Specifically, while directional data are relatively abundant for the Iberian Peninsula in the Roman period, intensity data and especially full-vector determinations are still rather scarce (Molina-Cardín et al., 2018).

A Roman pottery kiln in Calahorra (La Rioja) was used to carry out the first archaeointensity study in the Iberian Peninsula (Kovacheva et al., 1995). Later, the database was increased with 24 new archaeointensity data for the last 2000 yr by Gómez-Paccard et al., (2006, 2008). More recently, Hartman et al., (2009) contributed with 24 data from 1550 to 750 yr AD, being the first archaeointensity results from Portuguese pottery. Another 31 new data were obtained for the last three millennia during the last decade (Catanzariti et al., 2012; Osete et al., 2016). Molina-Cardín et al. (2018) have analysed 247 samples from fifteen different archaeological sites whose chronologies range between the 11th century BCE and the 19th century AD. Osete et al., (2020) have recently reported 14 new directional and 10 paleointensity results from 17 combustion structures (8th-5th centuries BCE) from the eastern part of Spain. Evans and Correia (2018) reported four new dates from Roman kilns in Portugal although based only on directional results. The number of paleointensity determinations in Iberia has significantly increased for the last 2-3 millennia including also the Roman period.

However, their quality is variable and not always fulfils quality criteria (Paterson et al., 2014) and / or they lack a good chronological control.

One reason for the limited availability of reliable paleointensity data are the difficulties inherent to palaeointensity experiments. The Thellier-type protocols are based on a set of assumptions that may not be fulfilled (e.g., Dunlop, 2011): a) the primary remanence must be a TRM; b) while the samples are heated during the experiments no chemical, mineralogical or physical changes in the samples should occur, because they will lead to erroneous paleointensity estimations (e.g., Thellier and Thellier, 1959); c) the samples must obey the Thellier laws of reciprocity, independence and additivity of partial thermoremanences (pTRM) acquired in intervals of temperature that do not overlap (Thellier and Thellier, 1959).

Another reason for inaccurate archaeointensity data is the absence of corrections for the anisotropy of thermoremanent magnetization (ATRM) and cooling rate (e.g. Palencia-Ortas et al., 2017). During the manufacture of archaeological samples, a preferred alignment of the ferromagnetic (*s.l.*) particles, specially on pottery, may significantly distort the magnetization record (Biedermann et al., 2019), generating discrepancies both in intensity and directional studies, with serious implications on the quality of the data and for archaeomagnetic dating purposes (e.g.: Osete et al. 2016; Palencia-Ortas et al. 2017).

In the present study, we have performed a full-vector archaeomagnetic determination on a Roman kiln to provide new high quality archaeomagnetic and archaeointensity data for the Iberian Peninsula during the Roman period (*ca.*218 BCE – 5th century AD (Pavón, 2019)). The studied kiln provides an extraordinary chance to obtain high quality data for the Iberian Peninsula dataset thanks to the very high accuracy of the

chronological control of the site, which is based on the pottery typology. The pottery found associated to the kiln presents a specific chronotypology, as *italic* and *gallic sigillata* that allows us to date the archaeological site and the kiln between 40 – 70 yr AD., thus yielding a very precise age date of 55 AD \pm 15 years (Bustamante and Detry, 2019).

2. MATERIAL AND METHODS

2.1 The archaeological site and the studied materials

In 2017 archaeologists re-started to excavate the north area of a Roman archaeological site called Mitreo's house in Mérida (Badajoz, Extremadura; Southwestern Spain; Figure 1a) (Bustamante and Detry, 2019), located in the Southern suburb of the capital of the Lusitania province. The renewed archaeological excavations began with the discovery of pottery fragments of local production, as “thinwalled” pottery, glazed pottery or common ware, from a previous phase of the construction of this *Domus*. To flatten the unevenness of the floor to build the house, pottery remains were placed onto the ground. Because of the finding of these potsherds at the beginning of this research, archaeologists had suggested that an artisanal installation dedicated to the production of pottery may have existed in the surrounding of the house. Later, an archaeological excavation started in the north area of the house during which a kiln was discovered (Figure 1a-b).

The kiln has a size of 2.48 x 2.48 meters. Its structure was delimited by “green bricks” which helped to isolate the kiln from the adjacent archaeological structures and the color oscillations made by the temperature changes. Despite the fact that many constructive elements of the house were built directly on top of the grill of the kiln, the structure is archaeologically very well preserved. The grill has a length is of 1.74 meters

and has ventilation openings like ducts (pipes that carry air out of the kiln). For the construction of the grill two master walls were built. “Green bricks” (28 x 21 x 7.5 centimeters) were put perpendicular to the master wall to build a mesh. The nozzle holes were raised on this lattice (Fig. 1b).

2.2 Archaeomagnetic sampling

The kiln was sampled collecting 11 independent hand blocks (~7cm x 7cm) and oriented with a magnetic compass and with the aid of plaster to ensure the highest accuracy and prevent the breakage of the samples. An horizontal surface was obtained on each hand block by dripping plaster of Paris and gently pressing a piece of methacrylate onto the plaster while wet and using bubble levels for levelling. Before removing each sample, a line pointing the magnetic North measured with a Brunton magnetic compass was drawn onto the dry plaster.

Samples were collected from the best burnt parts and from different parts of the kiln, to increase the significance of our results. Later, in the laboratory, the hand blocks were consolidated with sodium silicate and cut into cubic regular specimens (~2.2cm side length), always keeping the sampling orientation marks.

Also unoriented material obtained while cutting the hand blocks and associated to the latter was collected for absolute archaeointensity and rock-magnetic analyses.

[FIGURE 1]

2.3 Paleomagnetic and rock-magnetic analyses

All experiments were carried out at the paleomagnetic laboratory of Burgos University, Spain. The natural remanent magnetization (NRM) was measured with a 2G SQUID magnetometer (noise level $5 \times 10^{-12} \text{ Am}^2$). The magnetic susceptibility was measured at

room temperature initially and after each thermal demagnetization step using a KLY-4 susceptibility meter (AGICO; noise level 3×10^{-8} S.I) to detect the possible occurrence of mineralogical alterations during the experiments.

In order to correct the effect of local declination the latter was obtained from the World Magnetic Model (WMM) on the National Oceanic and Atmospheric Administration (NOAA) web page (<https://www.noaa.gov>). According to the site and the date, the difference between geographic and magnetic North is 1° W. The progressive demagnetization of NRM was performed both by stepwise thermal (TH) and alternating field (AF) demagnetization. Firstly, we carried out a pilot study to select the most appropriate demagnetization sequence. According to the results of the pilot study, the TH demagnetization was performed in 10 steps using a TD48 – SC (ASC) thermal demagnetizer. The AF demagnetization was carried out in 12 steps up to a maximum peak field of 100 mT, with a demagnetization unit included in the 2G magnetometer.

The direction of the characteristic remanent magnetization (ChRM) of all specimens was determined by principal component analysis (Kirschvink, 1980) including at least seven demagnetization steps and using the *Remasoft software* (Chadima y Hrouda, 2006). The mean paleomagnetic direction was calculated using Fisher (1953) statistics following a hierarchical averaging approach (Lanos et al. 2005). The hierarchical mean direction was first calculated averaging specimens of each hand-block and then all independently orientated hand-blocks.

The magnetic properties of the studied material were analysed with a Variable Field Translation Balance (MM_VFTB). The principal objective of these experiments is to identify the main magnetic carriers, their domain states and thermomagnetic stability and preselect the best samples for paleointensity experiments. The following experiments were performed: measurement of progressive isothermal remanent

magnetization (IRM) acquisition curves, hysteresis loops ($\pm 1\text{T}$), backfield curves and thermomagnetic magnetization vs. temperature ($M_s - T$) curves up to 700°C in air. All these experiments were carried out on powdered samples ($\sim 300\text{ mg}$) belonging to each of the 11 hand blocks sampled of the kiln.

Hysteresis parameters like the saturation of the remanent magnetization (M_{rs}), the saturation magnetization (M_s) and the coercive field (B_c) were obtained from the hysteresis cycles after correction for the paramagnetic fraction with the *Rock_Mag_Analyzer* software (Leonhardt, 2006). The coercivity of remanence (B_{cr}) was obtained from the backfield curves. Curie temperatures were determined from magnetization vs. temperature thermomagnetic curves with the two tangent method of Gromme et al. (1969).

2.4 Archaeointensity experiments

For archaeointensity experiments small irregular sample fragments were glued into 10 mm diameter borosilicate vials which had a carved orientation mark. Paleointensity determinations were carried out using a Thellier-type method (Thellier and Thellier, 1959) as modified by Coe (1967) in the paleomagnetic laboratory of Burgos University, Spain. The experiments were performed under air, using a TD48 – SC (ASC) thermal demagnetizer. The experiment was performed in eleven temperature steps from room temperature to 580°C . Temperature reproducibility between the two heating cycles at the same temperature could be held with a precision of $\pm 2^\circ\text{C}$. The laboratory field strength was set to $40\mu\text{T}$. Four control heatings (pTRM-checks) were carried out in order to check if mineralogical alterations occurred during the experiments. The first control heating was done after four heating steps (340°C) and subsequently, after each two heating steps (420 , 490 and 550°C). During the experiments, argon gas was used to minimize the possibility of having mineralogical alterations. Samples were left cooling

down naturally overnight and, for this reason, no extra measurements to correct for the cooling rate dependence of TRM were necessary (Calvo-Rathert et al., 2019). It is possible that this type of kilns had a cupola (e.g.: Cuomo Di Caprio, 2007), although there is no direct archaeological evidence in this case. However, experimental recreations indicate that the cooling of this type of kilns lasted several hours (e.g.: Coles 2014). A duration of some days cannot be completely excluded but is unlikely. Our cooling procedure tries to approach the natural cooling conditions as much as possible. Archaeological materials are often characterized by a non-negligible magnetic anisotropy of remanent magnetization (e.g., Aitken et al., 1981). For this reason, we corrected our archaeointensity determinations for TRM anisotropy by determining the anisotropy of TRM tensor (ATRM) and corrected our archaeointensity values following the method of Veitch et al. (1984) and using the *UmagPy* software (Tauxe et al., 2016). These measurements were carried out after completion of the palaeointensity experiments by inducing a pTRM (500°C to room temperature with a laboratory field strength of 40 μ T) in six sample directions (i.e. -x, +x, -z, +z, -y, +y) to sister specimens belonging to each of the studied hand blocks to ensure similar characteristics. Hand blocks have a small size, allowing the sampling of highly homogeneous archaeological material. This homogeneity in the magnetic properties is indicated also by some magnetic experiments like the thermomagnetic curves (Fig. 3) explained below. All samples were AF demagnetized at 100 mT before each pTRM acquisition and the remaining magnetization value was used as a baseline. Finally, an extra pTRM acquisition step was performed at the same field and temperature in the same direction than the first step in order to check if mineralogical changes had occurred during the anisotropy experiment.

3. RESULTS

3.1 Magnetic properties

Two different IRM acquisition curve types can be distinguished. While some samples are nearly saturated below 1 T (fig. 2a), others are still not saturated at this field (fig. 2b). Nevertheless, all have reached at least 90% saturation at 300mT (Fig. 2), showing the dominance of low coercivity minerals. Backfield curves yield B_{cr} values between 22 and 45 mT, also indicating that the magnetization is mainly carried by low coercivity minerals. Results are shown on Supplementary material Table 1.

[FIGURE 2]

Thermomagnetic curves (magnetization vs. temperature) were measured for 14 powdered samples. Each thermomagnetic curve includes a heating cycle up to 700°C and a cooling cycle. Two representative examples of curves are shown in Figure 3(a-b). The magnetization in both IRM and $M_s - T$ curves is dominated by a low coercivity fraction (magnetite), but also a high coercivity fraction (around 20% of magnetization) can be recognized in the IRM acquisition curves (Fig. 2). However, in the $M_s - T$ curves the magnetic signal of this high-coercivity phase is probably hidden by the main carrier (magnetite). Only a single ferromagnetic (*s.l.*) phase could be recognized in all cases, and its Curie temperature has been estimated around 570°C, suggesting that the main magnetic carrier is Ti-poor titanomagnetite. All curves showed a high degree of reversibility.

[FIGURE 3]

Results from thermomagnetic and IRM acquisition curves suggest that the remanence of the analyzed samples is mostly carried by magnetite. Although interpretation of results plotted in a Day diagram in terms of domain state analysis can be highly ambiguous, because hysteresis parameter ratios can be influenced by several conditions (Roberts et

al., 2018), the apparently simple composition of the samples from the present study may allow a qualitative interpretation. The observed hysteresis ratios (Supp. Fig. 1) vary between $0.30 \leq M_{rs}/M_s \leq 0.16$ and $1.94 \leq B_{cr}/B_c \leq 5.97$, suggesting that most of the samples lie in the pseudo-single domain (PSD) region. The dashed lines show that samples have a tendency towards SD + SP grains in the Day diagram (Supp. Fig. 1). Two of the samples have a high coercivity component in the IRM curves (Figure 2b), which would explain their shift to the right in the Day diagram (Fig. 1 Supp. Material). Hysteresis loops present both wasp-waisted and pot-bellied shapes. However, samples shifted to the right coincide with a wasp-waisted shape (Supp. Fig. 1c) due to the coexistence of magnetite and the high coercivity phase, most probably hematite given the reddish colour of the samples.

3.2 Archaeomagnetic directions

The Königsberger ratio Q_n (Königsberger, 1938; Stacey, 1967), is the ratio between remanent and induced magnetization [$Q_n = NRM / (\chi H)$], where χ is the magnetic susceptibility and H the intensity of the local magnetic field. This parameter can be useful to characterize burnt archaeological materials. It can be considered a measure of stability to indicate a rock's capability of maintaining a stable remanence.

In the present study, Q_n ratio values, (Fig. 4), vary between 5.19 and 25.05, indicating that the mechanism of magnetization has a thermal origin (TRM) (e.g.: Gómez-Paccard et al., 2012, Schnepf et al. 2004). Most samples are well clustered.

[FIGURE 4]

Archaeomagnetic directions were determined from thermally and AF-demagnetized specimens. All show a single normal-polarity component which is removed at 86 mT or 550°C. In addition, in all samples a very weak viscous component can be distinguished,

which is easily erased at fields below 17-23 mT (Fig. 5a-c) or temperatures below 200-300°C (Fig. 5d-e).

Figure 5f shows the directional results obtained from the analysis of 32 specimens from 8 different hand blocks. The directional results are detailed both at specimen and sample (block) level in supplementary Table 2. All analysed specimens provided reliable results and have been taken into account to calculate the hierarchical mean direction (Lanos et al. 2005): declination $D = 0.6^\circ$; inclination $I = 54.0^\circ$; precision parameter $k = 481$; α_{95} (radius of 95% confidence cone) = 2.5° . The studied kiln thus yields a reliable high-quality archaeomagnetic direction characterized by a very low scatter.

[FIGURE 5]

3.3 Archaeointensity results

28 fragments associated to seven hand blocks were preselected for paleointensity determination experiments. All analysed blocks showed a high directional stability and suitable rock magnetic properties. In the present study, absolute archaeointensity determinations were carried out with a Thellier-type double heating method (Thellier and Thellier, 1959) as modified by Coe (1967).

A paleointensity determination is accepted as reliable depending on a set of criteria to assess their quality, discarding those with evidence of the occurrence of alteration and/or the presence of remanence carried by multidomain (MD) grains. To assess the reliability of our samples, successful archaeointensity determinations had to fulfil the following requirements, which discriminate between two quality levels of different stringency, A and B:

- 1) At least five TRM-NRM points of the Arai plot (N) must be used for the paleointensity determination (both class A and B).

- 2) The ratio β ($\beta = \text{standard error/absolute slope of the slope of the best fit line}$) on the Arai diagram must be less than 0.1 (class A) and less than 0.15 (class B).
- 3) NRM fraction factor (f) (Coe et al., 1978) must be higher than 0.50 (class A) and 0.35 (class B).
- 4) The quality factor (q) (Coe et al., 1978) must be higher than 5 (class A) and higher than 1 (class B).
- 5) The maximum absolute difference observed in the pTRM check, normalized to the total TRM ($\delta(\text{ck})$, Leonhardt et al., 2000) must be less than 7 (class A) and less than 9 (class B).
- 6) Directions of NRM end-points at each step obtained in the zero-field steps of the experiment must draw a straight line pointing to the origin in the interval chosen for palaeointensity determination. Its mean angular deviation (MAD) must be less than 6 (class A) and less than 15 (class B).
- 7) The angular difference α between the free-floating data selected for palaeointensity determination (anchored to the centre of mass of the data) and the best-fit directions (anchored to the origin) must be less than 15° for both classes A and B. The directions of the natural remanent magnetization (NRM) obtained from Thellier-Coe experiments have to fall along a reasonably straight line.
- 8) Curvature (k') (Paterson, 2011) of the sector of the Arai plot selected for paleointensity determination should be less than 0.164 (quality level A) and less than 0.27 (quality level B).
- 9) In addition, at the site level, the threshold values require a standard deviation $\sigma_{\text{site}} \leq 15\%$ of the mean (Cromwell et al., 2015).

These criteria are all included in the ThellierTool criteria set (Leonhardt et al., 2004) except curvature k' (Paterson, 2011). Thresholds applied to the ThellierTool based criteria are mostly those proposed by Paterson (Paterson et al., 2014), except for fraction factor f . In this case, the original threshold $f \geq 0.5$ has been kept for class A determinations (instead of the lowered $f \geq 0.35$ value) while the modified threshold $f \geq 0.35$ has been accepted for class B determinations (instead of the $f \geq 0.30$ value of the original ThellierTool set).

Twenty-seven out of 28 samples (96.4%) yield successful determinations (Tab. 1). Figure 6 shows Arai plots of an accepted (a) and a rejected (b) determination. Between 9 and 12 TRM-NRM points of the Arai plot have been used in all cases. Fraction factor f varies between 0.53 and 1.01, and the quality factor q between 7.3 to 61.1. Only a single archaeointensity determination had to be rejected. Although all parameters fulfilled the aforementioned requirements, the obtained intensity value of 25 μT , was in complete disagreement with the remaining 27 samples (Tab. 1), which displayed rather homogeneous results so that we considered this determination as a rejected sample. At the site level, scatter is low with σ_{site} below 15% of the mean intensity. 12 samples fulfil class A (42.86%) and 15 fulfil class B (53.57%).

Before anisotropy correction, the mean archaeointensity value obtained from the 27 samples that have passed the selection thresholds, yields $F_{\text{NC}} = 57.7 \pm 3.9 \mu\text{T}$; ($58.0 \pm 2.0 \mu\text{T}$ if only class A determinations are considered).

ATRM experiments were carried out on new specimens from all blocks from which we had taken samples for archaeointensity experiments. One specimen from each block was analysed. In all investigated samples ATRM is low. The anisotropy factor varies between 0.90 and 1.04, and after ATRM correction, the corrected result yields a slightly

lower value $F_{ANIS} = 56.3 \pm 5.5 \mu\text{T}$; ($56.5 \pm 3.9 \mu\text{T}$ for class A determinations). Some archaeological samples such as pottery are very anisotropic because of their manufacture (e.g. Rogers et al., 1979; Veitch et al., 1984; Osete et al., 2016). However, the construction of a kiln usually implies less anisotropy because during its construction not so much manual pressure is necessary to mold and form it than as with potteries (e.g. Kovacheva et al., 2009).

[FIGURE 6]

[TABLE 1]

4. DISCUSSION

We have carried out an archaeomagnetic study in a kiln excavated in the archaeological site of Mitreo's house (Mérida, Spain). This study has allowed us to obtain a high quality full archaeomagnetic vector of the Earth's magnetic field from the Roman period. The hierarchical mean archaeomagnetic direction (Lanos et al., 2005) from 8 samples is the following: declination $D = 0.6^\circ$; inclination $I = 54.0^\circ$ ($k = 481$; $\alpha_{95} = 2.5^\circ$); the mean archaeointensity value after anisotropy correction is $56.3 \pm 5.5 \mu\text{T}$ (27 determinations of both class A and B); ($56.5 \pm 3.9 \mu\text{T}$ if only the 12 class A determinations are considered).

The kiln has associated pottery fragments, some of them providing an exceptionally well defined chronological control based on their characteristic typology. Indeed, while the general typology of the pottery associated with the kiln yields the 1st century AD, a rather wide chronological range, some of the fragments are of *italic* and *gallic sigillata* pottery; indicating a chronological interval from 40 to 70 AD. These are comparable with Drag. 30 type or local thin-walled as form Mayet XLIII / XLIV, XXXVII whose production started during the reign of Emperor Claudius (Bustamante, 2011). We can

also use the *ab silentio* criterium (Bustamante, 2011) with the absence of hispanic sigillata, of which trade started at the beginning of the Flavian dynasty, *ca.* 70 AD. The age interval of the kiln has been assigned to the age range of the pottery because of the relationship between them. Despite being a relative age determination, the well-constrained time interval allows us to include the full-vector data obtained into a SV curve or geomagnetic field model. Certainly, the obtained data are of high precision, both for the good quality magnetic data and for the excellent chronological constrain.

The high precision of the data obtained in the present study can be used to assess in how far models allow a reliable age determination. We have compared our mean direction and archaeointensity values with the SHA.DIF.14k geomagnetic field model (Pavón-Carrasco et al., 2014) using the *archaeo dating* software (Pavón-Carrasco et al., 2011), in order to check the quality of an archaeomagnetic dating using our results with the presently available geomagnetic data. We have selected this geomagnetic field model because it is based only on archaeomagnetic and lava flow data (excluding sedimentary data) for the last 14000 years. One of the limits of using PSVc for dating is the problem of the relocation error, which depends on the distance (Casas and Inconato, 2007). Conversely, the use of geomagnetic field models for archaeomagnetic dating prevents this error as synthetic secular variation curves are calculated at site coordinates (e.g.: Pavón-Carrasco et al. 2011). For this reason, the use of geomagnetic models is preferred as opposed to the standard archaeomagnetic dating based on regional SV curves, which are not always available for certain regions or contain gaps in their temporal distribution. According to the probability density function of the SHA.DIF.14k model, the last use of Mitreo's kiln was between 40 BC and 150 AD or between 290 AD and 516 AD, both at the 95% confidence level (Figure 7a). If we only use class A data for dating, ages between 65 BC and 158 AD or between 264

AD and 524 AD (95%) are obtained (Figure 7b). There is hardly any difference between using all or only type A data. Moreover, by using only type A data, the first interval is narrowed but the second one is extended.

The archaeological context suggests the 40 BC – 150 AD (95%) age interval (Figure 7a) or the 65 BC – 158 AD (95%) age interval if only class A results are used (Figure 7b) as the most plausible. On the other hand, despite the high quality of the data obtained, archaeomagnetic dating would only be able to give the rough estimation that probably the last time that the kiln was used was between the 1st and 2nd century AD.

[FIGURE 7]

The reason for this high uncertainty is related to the behavior of the Earth's magnetic field in the Iberian Peninsula during the Roman period and the low quality or scarcity of paleointensity data. Because the declination during this period shows a low variation, similar values are found both between the 1st and 2nd century AD and the 3rd to 5th century AD (Gómez-Paccard et al., 2006; 2013). Inclination, on the other hand, has three peaks intercalated with two minima (Molina-Cardín et al., 2018). Results of Palencia-Ortas et al., (2017) indicate the same behaviour as in our study, with minor fluctuations in declination between 300 BCE and 200 AD. However, around 200 AD the inclination decreases from 70° to 50° (Palencia-Ortas et al., 2017). Similarly, the intensity (Figure 7) value of the EMF observed between 400 BCE and 500 AD in the Iberia Peninsula shows hardly any variation, remaining around 60 μ T (Molina-Cardín et al., 2018) and hampering precise archeomagnetic dating in this time period.

Figure 8(a-c) shows archaeomagnetic directions and intensities from the Iberian Peninsula from 500 BCE to 500 AD (Geomagia 50.v3.3, Brown et al., 2015; Osete et al., 2020) together with the results from the present study shown in red. Blue squares

represent selected declination, inclination and intensity data from the Iberian Peninsula (updated Geomagia database, Brown et al., 2015; Osete et al., 2020) and black circles the declination, inclination and intensity data from the Iberian Peninsula (updated Geomagia database, Brown et al., 2015) not meeting selection criteria. During this period, declination does not show significant variation. However, data display a rather large scatter of nearly $\pm 20^\circ$ for the same age (Fig. 8a). Declination and age uncertainties are often large. Inclination data, on the other hand, exhibit a decrease after the 1st century (Fig. 8b), but this observation is overshadowed by an especially large uncertainty of data in this age range. Intensity data between approximately 400 BCE and 200 AD display a moderate drop (Fig. 8c). However, as with declinations, a large intensity scatter is observed for data of the same age, and age uncertainties are rather large.

Thus, directional and intensity data display a very high dispersion and large uncertainties (Figure 8a-c). We have compared the results from the present study with published data (Brown et al., 2015; Osete et al., 2020) applying specific selection criteria to take into account only those data which may present geomagnetic significance. The following criteria proposed by Molina-Cardin et al. (2018) were applied: (i) age error ≤ 250 years; (ii) more than 4 specimens had to be used to determine mean directions; (iii) $\alpha_{95} \leq 5.0^\circ$; (iv) paleointensity experiments must be based on Thellier-type methods with pTRM checks and TRM anisotropy correction for samples where it is necessary. Only 56 data remained after performing the selection. The selected data are also showed in Figure 8 for declination (a), inclination (b) and intensity (c). However, even after having performed the selection, declination presents a large scatter (Figure 8a) and inclination (Figure 8b) large uncertainties. In the selected

intensity data it is now possible to distinguish better (Figure 8c) the drop between 400 BCE and 200 AD, although with the same high uncertainties.

An increase of available high-quality full-vectors will thus help to sharpen the archeomagnetic dating tool and constrain the EMF's variations. A larger amount of high-quality data like those from the present study are necessary to improve the quality and resolution of the Iberian SVC, allowing to better discriminate between centuries during the Roman period in the Iberia Peninsula.

[FIGURE 8]

5. CONCLUSIONS

An archaeomagnetic and archaeointensity study was carried out on a kiln discovered in the archaeological site of Mitreo's house (Mérida, Spain). The age of the studied kiln is constrained with very high precision by the typology of pottery (*italic* and *gallic sigillata*) associated to the kiln, between 40 – 70 AD.

Our study has provided the following conclusions:

- 1) A well-defined high quality hierarchical mean archaeomagnetic field direction was obtained from 3 samples (32 specimens): declination $D = 0.6^\circ$; inclination $I = 54.0^\circ$; ($k = 401$; $\alpha_{95} = 2.5^\circ$).
- 2) Archaeointensity determinations were performed on 28 specimens using the Thellier – Coe protocol. Successful results were obtained on 27 specimens, with a success rate of 96.4%. The mean non-anisotropy corrected archaeointensity value obtained is $F = 57.7 \pm 3.9 \mu\text{T}$. If only paleointensity results of samples fulfilling a more stringent criteria set are considered (class A results) $F = 58.0 \pm 2.0 \mu\text{T}$.

- 3) Both the directional and intensity data obtained agree well with the variation observed in the Iberian PVS curve and regional databases, which exhibit a significant scatter for the Roman period.
- 4) Anisotropy of thermoremanent magnetization (ATRM) experiments were carried out to correct archaeointensity results for anisotropy effects. ATRM proved to be low (anisotropy factor $f = 0.90$ to 1.04). The mean anisotropy corrected archaeointensity value is $56.3 \pm 5.5 \mu\text{T}$ ($56.5 \pm 3.9 \mu\text{T}$ for class A specimens).
- 5) High-quality directional and intensity data along with an exceptional chronological data are reported. These type of results are very important to improve geomagnetic field databases in which the number of high quality full-vector data are very scarce. This is particularly important during the Roman period in the Iberian Peninsula because the small variation of the magnetic field vector components requires especially high-precision data to be able to perform reliable archaeomagnetic dating during this period.

6. ACKNOWLEDGEMENTS

This study was funded by the project BU235P18 of the Junta de Castilla y León and the European Regional Development Fund (ERDF), and project 10.13039/501100011033 of the Spanish State Research Agency (SRA). N-G.R acknowledges the financial support given by the Junta de Castilla y León and the European Union (ERDF funding). MCR acknowledges funding from the Fulbright Commission and the Spanish Ministry of Science, Innovation and Universities for a research stay at Hawaii University at Manoa. Thanks to the archaeological team who worked at the site. MBA acknowledges the following project: “Corpus Vasorum Hispanorum. Analisis tipológico, cronológico y prosopográfico de los sigilla en terra sigillata hispanica a partir de los centros

consumidores. Parte I: Lusitania” (PGC2018-093478-A-I00 – Convocatoria Proyectos de Excelencia – Plan Estatal de Generación de Conocimiento – Ministerio de Ciencia, Innovación y Universidades – España). Three anonymous reviewers are acknowledged for their constructive and helpful comments which improved the manuscript.

7. REFERENCES

- Aitken, M.J., Alcock, P.A., Bussell, G.D., and Shaw, C.J., 1981. Archaeomagnetic determination of the past geomagnetic intensity using ancient ceramics; allowance for anisotropy. *Archaeometry*, 23, 53-64.
- Biedermann, A.R., Bilardello, D., Jackson, M., Tauxe, L., Feinberg, J.M., 2019. Grain-size-dependent remanence anisotropy and its implications for paleodirections and paleointensities – Proposing a new approach to anisotropy corrections. *Earth Planet. Sci. Lett.* 512, 111–123. doi:10.1016/j.epsl.2019.01.051
- Brown, M.C., Donadini, F., Korte, M., Nilsson, A., Lodge, A., Lengyel, S., Korhonen, K., Constable, C.G., 2015. GEOMAGIA50.v3: 1. General structure and modifications to the archeological and volcanic database. *Earth Planets Space* 67, 83.
- Bustamante Álvarez, M., and Detry, C., 2019. Una oficina dedicada al tratamiento, manufactura y venta de objetos de hueso en Augusta Emerita. *Zephyrus*, LXXXIII, pp. 139-163.
- Bustamante, M. 2011: Nuevas consideraciones cronológicas en torno a la producción de paredes finas emeritenses, *Zephyrus*. LXVII, 161 - 170.
- Cai, S., Tauxe, L., Deng, C., Qin, H., Pan, Y., Jin, G., Chen, X., Chen, W., Xie, F., Zhu, R., 2016. New archaeomagnetic direction results from China and their

- constraints on palaeosecular variation of the geomagnetic field in Eastern Asia, *Geophysical Journal International*, Volume 207, Issue 2, 1332–1342, doi:10.1093/gji/ggw351
- Calvo-Rathert, M., Morales, J., Carrancho, A., Camps, P., Goguitchaichvili, A., Hill, M. J., 2019. Reproducibility of archaeointensity determinations with a multimethod approach on archaeological material reproductions. *Geophys. J. Int.* 218, 1719–1738.
- Calvo, M., Prevot, M., Perrin, M., 2001. Reasons for the failure of palaeointensity experiments: A study on historical lava flows from Mt. Etna. *Gji in press*, 44–63.
- Carrancho, Á., Goguitchaichvili, A., Morales, J.I., Espinosa, J.A., Villalaín, J.J., Arsuaga, J.L., Baquedano, E., Pérez-González, A. 2017. Full-Vector Archaeomagnetic Dating of a Medieval Limekiln at Pinilla Del Valle Site (Madrid, Spain). *Archaeometry* 59, 373 – 394.
- Carrancho A, Villalaín JI, Pavón-Carrasco FJ, Osete ML, Straus LG, Vergès JM, Carretero JM, Angelucci DE, González-Morales MR, Arsuaga JL, Bermúdez de Castro JM, Carbonell E, 2013. First directional European palaeosecular variation curve for the Neolithic based on archaeomagnetic data. *Earth Planet. Sci. Lett.* 380: 124–137. doi:10.1016/j.epsl.2013.08.031
- Casas, Ll. and Tema, E., 2019. Investigating the expected archaeomagnetic dating precision in Europe: A temporal and spatial analysis based on the SCHA.DIF.3K geomagnetic field model. *Journal of Archaeological Science* 108, 104972. doi:10.1016/j.jas.2019.104972
- Casas, L., Auguet, C., Cantoni, G., Vilar, J.L., Guasch, N., Prevosti, M., 2018. Using

- archaeomagnetism to improve the dating of three sites in Catalonia (NE Spain). *J. Cult. Herit.* 31, 152–161. doi:10.1016/j.culher.2017.11.004
- Casas, L., Prevosti, M., Fouzai, B., Álvarez, A., 2014. Archaeomagnetic study and dating at five sites from Catalonia (NE Spain), In *Journal of Archaeological Science*, Volume 41, 856-867, doi:10.1016/j.jas.2013.10.020
- Casas, L., Incoronato, A., 2007. Distribution analysis of errors due to relocation of geomagnetic data using the “Conversion via Pole” (CVP) method: Implications on archaeomagnetic data. *Geophys. J. Int.* 169, 448–454. doi:10.1111/j.1365-246X.2007.03346.x
- Catanzariti, G., Gómez-Paccard, M., McIntosh, G., Favón-Carrasco, F.J., Chauvin, A., Osete, M.L., 2012. New archaeomagnetic data recovered from the study of Roman and Visigothic remains from central Spain (3rd-7th centuries). *Geophys. J. Int.* 188, 979–993.
- Chadima and Hrouda, 2006. *ROMASOFT 3.0*. *Trav. Géophysiques XXVII*, 20–21.
- Coe, R.S., Grommé, S., Mankinen, E.A., 1978. Geomagnetic paleointensities from radiocarbon-dated lava flows on Hawaii and the question of the Pacific non-dipole low. *J Geophys Res* 83(B4):1740–1756. doi:10.1029/JB083iB04p01740
- Coe, R. S., 1967. Paleointensities of the earth’s magnetic field determined from Tertiary and Quaternary rocks, *J. Geophys. Res.*, 72 (12), 3247-3262, doi:10.1029/JZ072i012p03247.
- Coles, J. 2014. *Archaeology by experiment*. Routledge Library Edition. Taylor & Francis Ltd. London, UK. 192 pp.
- Cromwell, G., Tauxe, L., Halldórsson, SA., 2015. New paleointensity results from rapidly cooled Icelandic lavas: Implications for Arctic geomagnetic field strength.

Journal of Geophysical Research: Solid Earth Volume 120, Issue 5

- Cuomo Di Caprio N., 2007, *Ceramica in archeologia 2. Antiche tecniche di lavorazione e moderni metodi d'indagine*, L'Erma di Bretschneider, Roma.
- De Marco, E., Spassov, S., Kondopoulou, D., Zananiri, I., Gerofoka, E., 2008. Archaeomagnetic study and dating of a Hellenistic site in Katerini (N. Greece). *Phys. Chem. Earth* 33, 481–495. doi:10.1016/j.pce.2008.02.017
- Dunlop, D. 2011. Physical basis of the Thellier-Thellier and related paleointensity methods. *Phys. Earth Planet. Int.*, 187(3):118-138, DOI: 10.1016/j.pepi.2011.03.006
- Dunlop, D.J., 2002. Theory and application of the Day plot (Mrs/Ms versus Hcr/Hc) 1. Theoretical curves and tests using titanomagnetite data. *J. Geophys. Res.* 107, EPM4-1-EPM4-22. doi:10.1029/2001JG001486
- Evans, M. E., and Correia, A., 2018. Archaeomagnetism of four pottery kilns in central Portugal: Implications for secular variation and dating. *Open Journal of Archaeometry* 4: 7171, 5 pp. DOI: 10.4081/arc.2018.7171
- Fisher, R., 1953. Dispersion on a Sphere. *Proc. R. Soc. A Math. Phys. Eng. Sci.* 217, 295–305. doi:10.1098/rspa.1953.0064
- Gallet, Y., Genevey, A., Le Goff, M., 2002. Three millennia of directional variation of the Earth's magnetic field in western Europe as revealed by archaeological artefacts. *Phys Earth Planet Inter* 131:81–89.
- García-Redondo, N., Carrancho, Á., Goguitchaichvili, A., Morales, J., Calvo-Rathert, M., Palomino, A., 2020. New constraints on the medieval repopulation process in the northern Iberian plateau from the full vector archaeomagnetic dating of two hearths at La Pudia site (Caleruega, Burgos, Spain). *Archaeol Anthropol Sci* 12, 91. doi:10.1007/s12520-020-01041-1

- García-Redondo, N., Carrancho, Á., Goguitchaichvili, A., Morales, J., Palomino, A., 2019. Comprehensive magnetic surveys of kilns for bell and tile fabrication in Castile (Spain). *J Archaeol Sci Rep* 23: 426–436. doi:10.1016/j.jasrep.2018.11.003
- Gómez-Paccard, M., Beamud, E., Mc Intosh, G., Larrasoaña, J.C., 2013. New archaeomagnetic data recovered from the study of three roman kilns from north-east Spain: A contribution to the Iberian palaeosecular variation curve. *Archaeometry* 55, 159–177. doi:10.1111/j.1475-4754.2012.00675.x
- Gómez-Paccard, M., Chauvin, A., Lanos, P., Dufresne, P., Kovacheva, M., Hill, M.J., Beamud, E., Blain, S., Bouvier, A., Guibert, P., 2012. Improving our knowledge of rapid geomagnetic field intensity changes observed in Europe between 200 and 1400 AD. *Earth Planet. Sci. Lett.* 355–356, 131–143. doi:10.1016/j.epsl.2012.08.037
- Gómez-Paccard, M., Chauvin, A., Lanos, P., Thiriot, J., 2008. New archeointensity data from Spain and the geomagnetic dipole moment in western Europe over the past 2000 years. *Journal of Geophysical Research: Solid Earth*, Volume 13. doi:10.1029/2008JB005082.
- Gómez-Paccard, M., Chauvin, A., Lanos, P., Thiriot, J., Jiménez-Castillo, P., 2006. Archeomagnetic study of seven contemporaneous kilns from Murcia (Spain). *Phys. Earth Planet. Inter.* 157, 16–32. doi:10.1016/j.pepi.2006.03.001
- Gromme, C.S., Wright, T.L., Peck, D.L., 1969. Magnetic Properties And Oxidation Of Iron-Titanium Oxide Minerals In Alae And Makaopuhi Lavalakes, Hawaii. *J. Geophys. Res.* 74, 5277.
- Hartmann, G.A., Trindade, R.F., Goguitchaichvili, A., Etchevarne, C., Morales, J., Afonso, M.C., 2009. First archeointensity results from Portuguese potteries (1550–

- 1750 AD). *Earth Planets Space* 61 (1): 93–100
- Hervé, G., Lanos, P., 2018. Improvements in archaeomagnetic dating in western Europe from the late bronze to the late iron ages: an alternative to the problem of the Hallstattian radiocarbon plateau. *Archaeometry*, 60 (4), 870-883.
- Hervé, G., Chauvin, A., Lanos, P., 2013. Geomagnetic field variations in Western Europe from 1500 BC to 200 AD. Part I: directional secular variation curve. *Phys Earth Planet Inter* 218:1–13. doi:10.1016/j.pepi.2013.02.003
- Kirschvink, J.L., 1980. The least-square line and plane and the analysis of paleomagnetic data. *Geophys. J. R. Astron. Soc.* 62, 699–718.
- Königsberger, J.G. 1938. Natural residual magnetism of eruptive rocks: *Terrestrial Magnetism Atmospheric Electricity*, 43, 299 – 320.
- Kostadinova-Avramova, M. and Kovacheva, M., 2015. Further studies on the problems of geomagnetic field intensity determination from archaeological baked clay materials. *Geophys. J. Int.* 203, 588–604. doi: 10.1093/gji/ggv310
- Kovacheva, M., Kostadinova-Avramova, M., Jordanova, N., Lanos, P., Boyadzhiev, Y., 2014. Extended and revised archaeomagnetic database and secular variation curves from Bulgaria for the last eight millennia, *Physics of the Earth and Planetary Interiors*, Volume 236, Pages 79-94. doi:10.1016/j.pepi.2014.07.002.
- Kovacheva, M. Chauvin, A., Jordanova, N., Lanos, P., 2009. Remanence anisotropy effect on the palaeointensity results obtained from various archaeological materials, excluding pottery. *Earth Planets and Space* 61(6):711-732. DOI: 10.1186/BF03353179

- Kovacheva, M., Parés, J.M., Jordanova, N., Karloukovski, V., 1995. A new contribution to the archaeomagnetic study of a Roman pottery kiln from Calahorra (Spain). *Geophysical Journal International*, Volume 123, Issue 3, 931–936, doi:10.1111/j.1365-246X.1995.tb06899.x
- Lanos P, Le Goff M, Kovacheva M, Schnepf E., 2005. Hierarchical modelling of archaeomagnetic data and curve estimation by moving average technique. *Geophys. J. Int.* 160: 440–476. doi:10.1111/j.1365-246X.2005.02490.x
- Leonhardt, R., 2006. Analyzing rock magnetic measurements: The RockMagAnalyzer 1.0 software. *Comput. Geosci.* 32, 1420–1431. doi:10.1016/j.cageo.2006.01.006
- Leonhardt, R., Heunemann, C. Krasa, D., 2006. Analyzing absolute paleointensity determinations: acceptance criteria and the software ThellierTool 4.0, *Geochem. Geophys. Geosyst.*, 5, Q12016, doi:10.1029/2004GC000807.
- Leonhardt, R., Hufenbecher, F., Heider, F., Soffel, H., 2000. High absolute paleointensity during a mid-Miocene excursion of the Earth's magnetic field, *Earth Planet. Sci. Lett.*, 184, 141–154.
- Molina-Cardín, A., Campuzano, S.A., Osete, M.L., Rivero-Montero, M., Pavón-Carrasco, F.J., Palencia-Ortas, A., Martín-Hernández, F., Gómez-Paccard, M., Chauvin, A., Guerrero-Suárez, S., Pérez-Fuentes, J.C., McIntosh, G., Catanzariti, G., Sastre Blanco, J.C., Larrazabal, J., Fernández Martínez, V.M., Álvarez Sanchís, J.R., Rodríguez-Hernández, J., Martín Viso, I., Garcia i Rubert, D., 2018. Updated Iberian Archeomagnetic Catalogue: New Full Vector Paleosecular Variation Curve for the Last Three Millennia. *Geochemistry, Geophys. Geosystems* 19, 3637–3656. doi:10.1029/2018GC007781
- Osete, M.L., Molina-Cardín, A., Campuzano, S.A., Aguilera-Arzo, G., Barrachina-

- Ibáñez, A., Falomir-Granell, F., Oliver Foix, A., Gómez-Paccard, M., Martín-Hernández, F., Palencia-Ortas, A., Pavón-Carrasco, F.J., Rivero-Montero, M., 2020. Two archaeomagnetic intensity máxima and rapid directional variation rates during the Early Iron Age observed at the Iberian coordinates. Implications on the evolution of the Levantine Iron Age Anomaly. *Earth and Planetary Science Letters* 533, 116047.
- Osete, M.L., Chauvin, A., Catanzariti, G., Jimeno, A., Campuzano, S.A., Benito-Batanero, J.P., Taberner-Galán, C., Roperch, P., 2015. New archaeomagnetic data recovered from the study of celtiberic remains from central Spain (Numantia and Ciadueña, 3rd-1st BC). Implications on the fidelity of the Iberian palaeointensity database. *Phys. Earth. Planet. Inter.* 260, 74–86.
- Oyamburu, L., Villalaín, J.J., Osete, M.L., Zarzalejos, M., Blasco, C. 1995. Estudio paleomagnético del yacimiento de Villa del Pañuelo (Villamanta, Madrid). *Geogaceta*, 20 (5), 1044-1046.
- Palencia-Ortas, A., Osete, M.L., Campuzano, S.A., McIntosh, G., Larrazabal, J., Sastre, J., Rodríguez-Aranda, J. 2017. New archaeomagnetic directions from Portugal and evolution of the geomagnetic field in Iberia from Late Bronze Age to Roman Times. *Phys. Earth Planet. Inter.* 270, 183–194. doi:10.1016/j.pepi.2017.07.004
- Parés, JM., De Jonge, R., Pascual, JO., Bermúdez, A., Tovar, CJ., Luezas, RA., Maestro, N. 1992. Archaeomagnetic evidence for the age of a Roman pottery kiln from Calahorra (Spain). *Geophys. J. Int.* 112, 533-537.
- Paterson, G. A., L. Tauxe, A. J. Biggin, R. Shaar, and L. C. Jonestrask, 2014. On improving the selection of Thellier- type paleointensity data, *Geochem. Geophys. Geosyst.*, 15, 1180–1192, doi:10.1002/2013GC005135.

- Pavón, P., 2019. "Aproximación a la implantación del dominio romano", Sánchez López, E.H. y Bustamante-Álvarez, M. (eds.) *Arqueología Romana de la Península Ibérica*, Editorial Universidad de Granada, Granada, 65-78.
- Pavón-Carrasco, F.J., Gómez-Paccard, M., Hervé, G., Osete, M.L., Chauvin, A., 2014. Intensity of the geomagnetic field in Europe for the last 3 ka: Influence of data quality on geomagnetic field modeling. *Geochemistry, Geophys. Geosystems* 15, 2515–2530. doi:10.1002/2014GC005311
- Pavón-Carrasco, F.J., Osete, M.L., Torta, J.M., De Santis, A., 2014. A geomagnetic field model for the Holocene based on archaeomagnetic and lava flow data. *Earth Planet. Sci. Lett.* 388, 98–109. doi:10.1016/j.epsl.2013.11.046
- Pavón-Carrasco, F.J., Rodríguez-González, J., Osete, M.L., Torta, J.M., 2011. A Matlab tool for archaeomagnetic dating. *J. Archaeol. Sci.* 38, 408–419. doi:10.1016/j.jas.2010.09.021
- Pavón-Carrasco, F.J., Osete, M.L., Torta, J.M., 2010. Regional modeling of the geomagnetic field in Europe from 6000 to 1000 B.C. *Geochemistry, Geophys. Geosystems* 11, 1–20. doi:10.1029/2010GC003197
- Pavón-Carrasco, F.J., Osete, M.L., Torta, J.M., Gaya-Piqué, L.R., 2009. A regional archeomagnetic model for Europe for the last 3000 years, SCHA.DIF.3K: applications to archeomagnetic dating. *Geochem. Geophys. Geosyst.* 10 (Q03013). doi:10.1029/2008GC002244
- Roberts, A.P., Tauxe, L., Heslop, D., Zhao, X. and Jiang, Z.X., 2018. A critical appraisal of the “Day Diagram”. *J. Geophys. Res.: Solid Earth*, vol. 123, no. 4, pp. 2618-2644. doi: 10.1002/2017JB015247

- Rogers, J., J. M. W. Fox, and M. J. Aitken, Magnetic anisotropy in ancient pottery, *Nature*, 277(5698), 644–646, 1979.
- Ruiz-Martínez, V.C., Pavón-Carrasco, F.J., Catanzariti, G., 2008. First archaeomagnetic data from northern Iberia, *Physics and Chemistry of the Earth*. Volume 33, Issues 6–7, 566-577. doi:10.1016/j.pce.2008.02.023
- Schnepf, E., Thallner, D., Arneitz, P., Mauritsch, H., Scholger, R., Rolf, C., Leonhardt, R., et al., 2020. New archaeomagnetic secular variation data from Central Europe. I: directions. *Geophys. J. Int.* (2020) 220, 1023–1044
- Schnepf, E., Lanos, Ph., 2005. Archaeomagnetic secular variation in Germany during the past 2500 years. *Geophys. J. Int.* 163, 479–489.
- Schnepf, E., Pucher, R., Reinders, J., Harpach, U., Soffel, H. and Hedley, I., 2004. A German catalogue of archaeomagnetic data. *Geophysical Journal International*, 157: 64-78. doi:10.1111/j.1365-246X.2004.02163.x
- Stacey, F.D. 1967. The koenigsberger ratio and the nature of thermoremanence in igneous rocks. *Earth planet. Sci. Lett.*, 2, 67–68.
- Tauxe, L., Shaar, N., Jones-trask, L., Swanson-Hysell, NL., Minnett, R., Koppers, AAP., Constable, CG., Jarboe, N., Gaastra, K., and Fairchild, L., 2016. PmagPy: Software package for paleomagnetic data analysis and a bridge to the Magnetics Information Consortium (MagIC) Database, *Geochem. Geophys. Geosyst.*, 17, doi:10.1002/2016GC006307.
- Tema, E. Fantino, F., Ferrara, E., Lo Giudice, A., Morales, J., Goguitchaichvili, A., Camps, P., Barelli, F., Gulmini, M., 2013. Combined archaeomagnetic and thermoluminescence study of a brick kiln excavated at Fontanetto Po (Vercelli,

Northern Italy). *J. Archaeol. Sci.* 40 (4), 2025–2035.

Tema, E., Kondopoulou, D., 2011. Secular variation of the Earth's magnetic field in the Balkan region during the last 8 millennia based on archaeomagnetic data. *Geophys. J. Int.* 186, 603-614.

Theilner, E., Theilner, O., 1959. Sur l'intensité du champ magnétique terrestre dans le passé historique et géologique. *Ann. Geophys.* 15, 285–376.

Veitch, J., Hedley, I. and Wagner, J.J., 1984. An investigation of the intensity of the geomagnetic field during roman times using magnetically anisotropic bricks and tiles. *Archeological Sciences, Geneva* 37: 359-373.

Figure captions

Figure. 1. Map of the Iberian Peninsula with the location of Mitreo's house archaeological site and the kiln sampled for this study.

Figure 2. (a-b) Normalized progressive IRM acquisition curves up 1 T of representative samples. Figure 2b shows examples where the high-coercivity contribution is more easily detected.

Figure 3. (a-b) Representative thermomagnetic curves. Heating (cooling) cycles are indicated in red (blue) with their respective arrows. Sample codes and magnetization intensities are indicated.

Figure 4. Königsberger ratio (Q_n) diagram showing NRM intensity (A/m) versus bulk magnetic susceptibility values. Königsberger ratio isolines indicating constant Q_n values from 0.1 to 1000 are shown.

Figure 5. Representative orthogonal NRM demagnetization diagrams showing the behavior during (a, b and c) alternating field and (d and e) thermal demagnetization.

Green (blue) symbols represent the vertical (horizontal) projections of vector endpoints. Sample code, initial NRM intensity values and main demagnetization steps are shown. (f) Equal-area projection showing all ChRM directions, with the mean hierarchical direction and the α_{95} confidence circle (in red). n/N , number of samples considered/analysed; Dec., declination; Inc., inclination; k , precision parameter; α_{95} , semi-angle of confidence.

Figure 6. (a-b) Two representative examples of accepted (a) and rejected (b) Thellier-Coe archaeointensity experiments. The NRM-TRM diagrams are shown with orthogonal vector projections of the remanent magnetization (Zijderveld diagrams) and with M-T plot.

Figure 7. Probability of age density functions obtained with the MATLAB tool from Pavón-Carrasco et al. (2011) comparing the SHA.DIF.14k model with the declination, inclination and intensity values at site coordinates from the kiln studied. Results are expressed at 95% probability. (a) includes intensity class A and B; (b) includes intensity class A.

Figure 8. Archaeomagnetic data (declination (a), inclination (b) and intensity (c)) in the Iberian Peninsula between 500 BC and 500 AD. (Geomagia 50.v3.3, Brown et al., 2015). Osete et al., 2020. Red squares: Results from the present study. In the intensity plot, mean results of both type A determinations and all successful determinations (types A and B) are shown. Both means are virtually indistinguishable. Blue squares: Selected declination, inclination and intensity data from the Iberian Peninsula (updated Geomagia database, Brown et al., 2015; Osete et al., 2020) (see text). Black circles: Declination, inclination and intensity data from the Iberian Peninsula (updated Geomagia database, Brown et al., 2015) not meeting selection criteria. The selected published data correspond to the following studies: Carrancho et al. 2013; Casas et al.

2014; Gómez-Paccard et al. 2006; 2008; 2013; Kovacheva et al. 1995; Molina-Cardín et al. 2018; Osete et al. 2016; 2020; Oyamburu et al. 1996; Palencia-Ortas et al. 2017; Parés et al. 1992; Ruiz et al. 2008.

Journal Pre-proof

Table 1.

| SPECIMEN | CLASS | N | T _{min} -T _{max} | f | β | δck | k' | q | MAD | α | B _{raw} [μT] | B _{An corr} [μT] |
|---------------|-------|----|------------------------------------|------|-------|------|--------|-------|------|-------------------|--------------------------|------------------------------|
| CM1-9 | B | 11 | 0-550 | 0.77 | 0.05 | 4.26 | 0.164 | 12.52 | 8.1 | 1.75 | 50.5 | 48.48 |
| CM1-10 | B | 10 | 0-520 | 0.53 | 0.06 | 4.32 | 0.054 | 7.31 | 9.4 | 9.40 | 51.9 | 49.82 |
| CM1-11 | B | 11 | 0-550 | 0.76 | 0.051 | 4.44 | 0.145 | 12.54 | 10.7 | 3.35 | 52.5 | 50.4 |
| CM1-12 | B | 11 | 0-550 | 0.8 | 0.035 | 3.71 | -0.018 | 19.33 | 6.8 | 2.04 | 53.3 | 51.16 |
| CM3-13 | B | 11 | 0-550 | 0.94 | 0.022 | 7.85 | -0.125 | 37.18 | 8.7 | 1.21 | 65.5 | 68.12 |
| CM3-14 | B | 12 | 0-580 | 1.01 | 0.029 | 7.24 | 0.03 | 30.51 | 4.1 | 0.18 | 57.2 | 59.48 |
| CM3-15 | B | 12 | 0-580 | 1 | 0.025 | 4.08 | 0.191 | 34.13 | 2.8 | 0.52 | 59 | 61.36 |
| CM3-16 | B | 12 | 0-580 | 0.99 | 0.019 | 5.46 | 0 | 44.95 | 7.2 | 1.74 | 64.6 | 67.18 |
| CM5-17 | B | 12 | 0-580 | 0.96 | 0.038 | 5.26 | 0 | 22.52 | 6.3 | 2.68 | 55.4 | 52.07 |
| CM5-18 | B | 12 | --- | 1 | 0.018 | 3.98 | 0 | 50.19 | 5.2 | 1.45 | 25.1 | Rejected |
| CM5-19 | A | 12 | 0-580 | 0.99 | 0.029 | 5.82 | 0.053 | 29.79 | 4.6 | 1.66 | 60.4 | 56.77 |
| CM5-20 | B | 10 | 0-520 | 0.88 | 0.044 | 1.80 | -0.178 | 16.86 | 2.6 | 1.08 | 52.8 | 49.63 |
| CM7-21 | A | 12 | 0-580 | 0.97 | 0.027 | 4.48 | 0 | 51.41 | 2.8 | 0.86 | 53.2 | 47.88 |
| CM7-22 | B | 12 | 0-580 | 0.96 | 0.035 | 6.13 | 0 | 24.07 | 7.5 | 2.27 | 59.9 | 53.91 |
| CM7-23 | A | 12 | 0-580 | 0.97 | 0.018 | 4.54 | 0.003 | 17.69 | 5.9 | 2.15 | 58.1 | 52.29 |
| CM7-24 | B | 12 | 0-580 | 0.94 | 0.061 | 5.56 | 0 | 13.69 | 11.2 | 3.98 | 56.6 | 50.94 |
| CM9-25 | A | 12 | 0-580 | 0.99 | 0.018 | 4.74 | 0.165 | 47.71 | 4.2 | 1.12 | 59.7 | 57.90 |
| CM9-26 | B | 12 | 0-580 | 0.98 | 0.054 | 7.00 | 0 | 15.64 | 7.5 | 1.65 | 66 | 64.02 |
| CM9-27 | A | 12 | 0-580 | 0.98 | 0.028 | 6.20 | 0 | 31.37 | 5.1 | 1.23 | 57.7 | 55.96 |
| CM9-28 | A | 12 | 0-580 | 0.99 | 0.019 | 6.65 | 0 | 44.97 | 4.4 | 0.57 | 60.2 | 58.39 |
| CM10-29 | A | 12 | 0-580 | 0.99 | 0.014 | 4.26 | 0.029 | 61.14 | 3.1 | 0.83 | 60.3 | 62.71 |
| CM10-30 | B | 9 | 0-491 | 0.78 | 0.08 | 5.97 | 0 | 8.08 | 11.8 | 1.96 | 56.2 | 58.44 |
| CM10-31 | A | 12 | 0-580 | 0.98 | 0.027 | 5.77 | -0.058 | 30.91 | 4.6 | 1.21 | 58 | 60.32 |
| CM10-32 | A | 12 | 0-580 | 0.99 | 0.017 | 5.72 | 0.008 | 52.51 | 3.9 | 0.96 | 58.1 | 60.42 |
| CM11-33 | A | 12 | 0-580 | 0.97 | 0.022 | 3.06 | -0.054 | 38.9 | 5 | 1.79 | 56.4 | 54.71 |
| CM11-34 | B | 12 | 0-580 | 0.99 | 0.021 | 8.76 | -0.012 | 41.16 | 5.6 | 2.08 | 60.2 | 58.39 |
| CM11-35 | A | 12 | 0-580 | 0.95 | 0.031 | 4.01 | -0.15 | 27.12 | 4.8 | 1.90 | 57.9 | 56.16 |
| CM11-36 | A | 12 | 0-580 | 0.95 | 0.038 | 3.70 | 0 | 21.99 | 4.4 | 1.59 | 56.9 | 55.19 |
| Mean = | | | | | | | | | | 57.7 ± 3.9 | 56.3 ± 5.5 | |

Table 1. Archaeointensity data for the studied specimens. Specimen: name of the specimen; Class (see text), N: number of data points within this temperature interval; T_{min}-T_{max}: interval temperature used for the slope calculation; f: fraction of NRM used for the slope calculation; β: the ratio of the standard error of the slope to the absolute value of the slope; δck: alteration factor; k': curvature factor; q: quality factor; MAD: the maximum absolute difference produced by a pTRM check, normalized by the total TRM; α: the angular difference between the anchored and free best-fit directions; B_{raw}: uncorrected intensity value before anisotropy corrections; B_{An corr}: intensity value corrected for anisotropy effects.

N. García-Redondo: Investigation, Formal Analysis, Validation, Writing - Original Draft, Writing - Review & Editing, Visualization.

M. Calvo-Rathert: Conceptualization, Validation, Writing - Review & Editing, Supervision, Project administration, Funding acquisition.

A. Carrancho: Conceptualization, Validation, Writing - Review & Editing, Supervision, Project administration, Funding acquisition.

M. Bustamante-Álvarez: Resources, Writing - Review & Editing, Project administration.

Journal Pre-proof

HIGHLIGHTS

- New high quality full-vector archaeomagnetic data from a Roman kiln in Spain.
- Exceptional archaeointensity success rate (96%) on 27 specimens with Thellier method.
- Well constrained typological pottery dating (40-70 AD) confirmed with archaeomagnetism.
- A new high-quality result for Iberian archaeomagnetic database is reported.

Journal Pre-proof



Figure 1

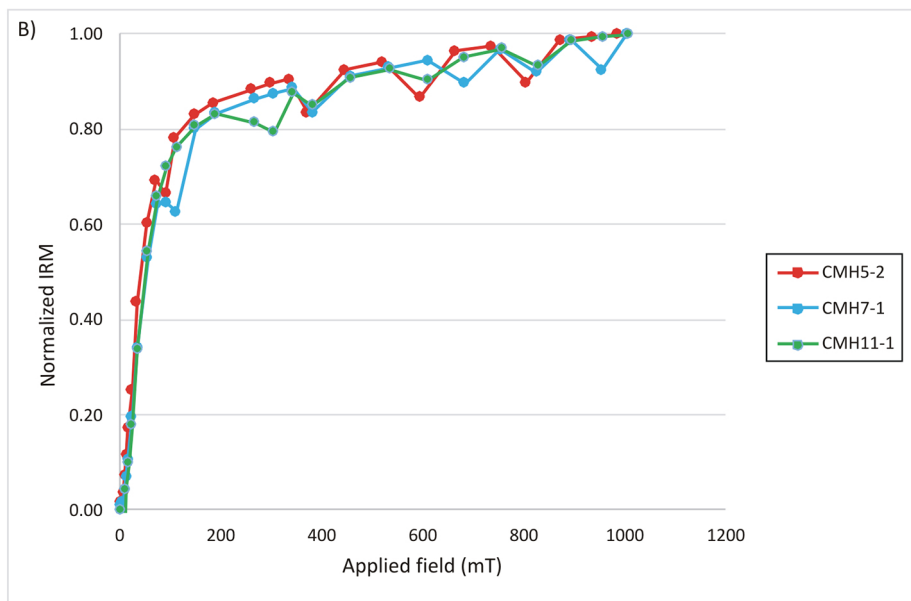
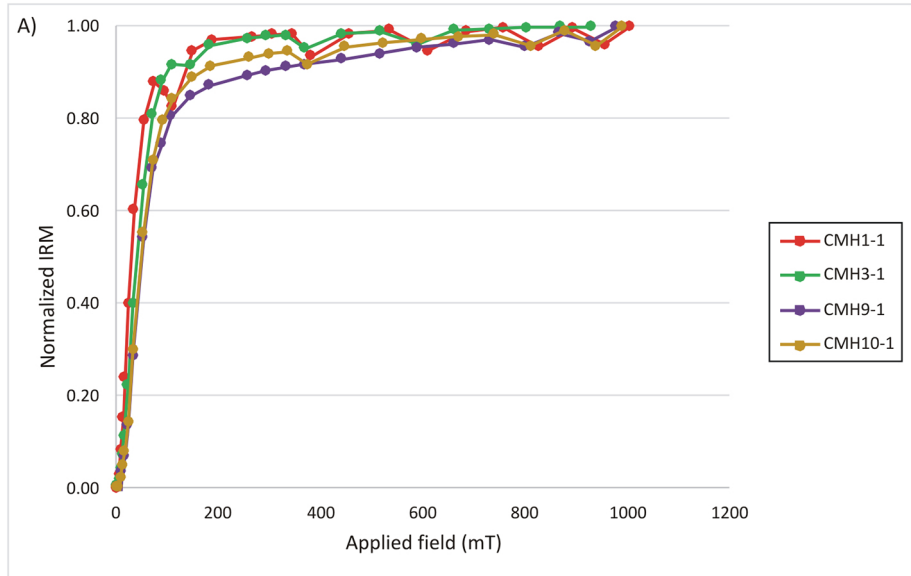


Figure 2

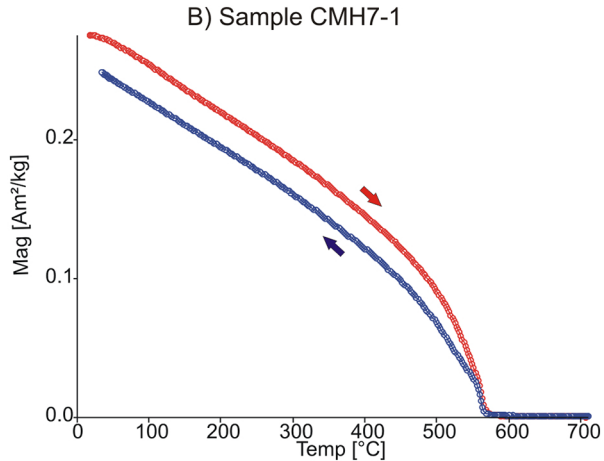
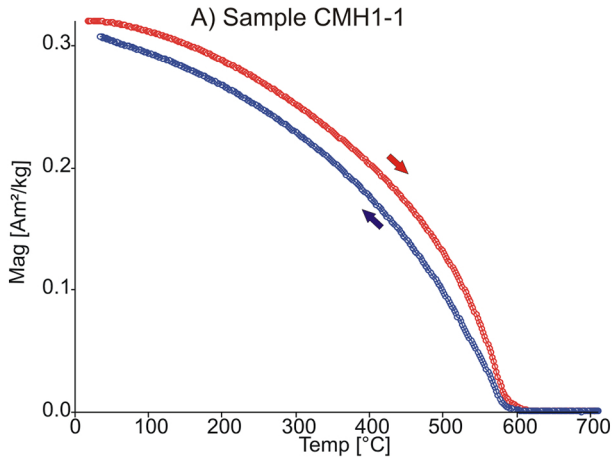


Figure 3

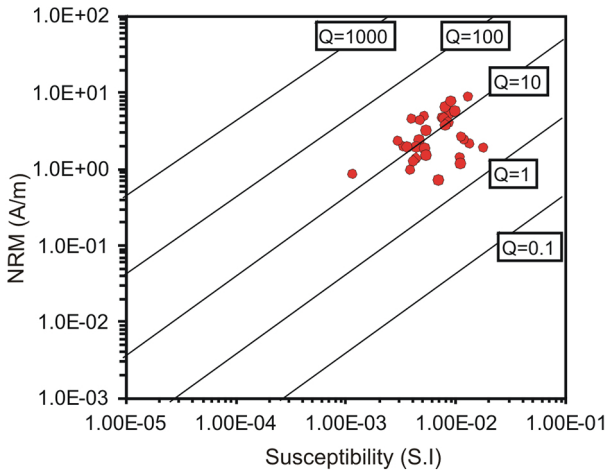


Figure 4

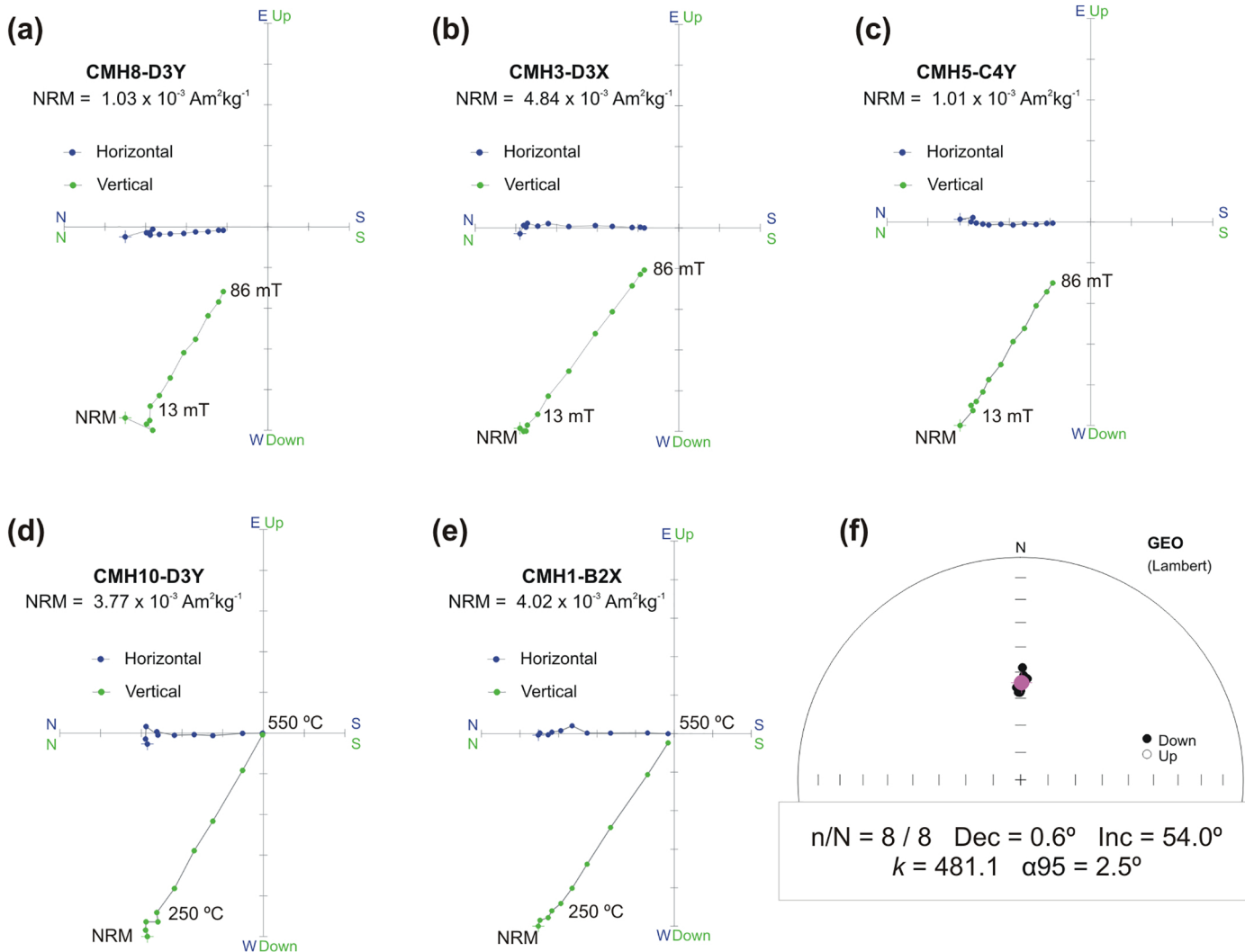
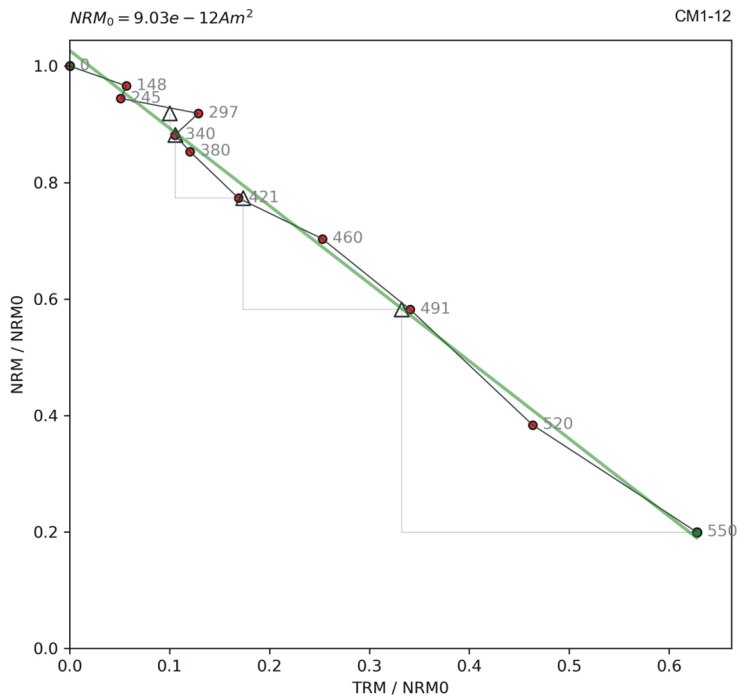


Figure 5

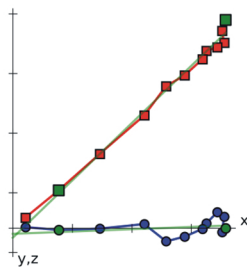
A) Sample CM1-12

Arai plot



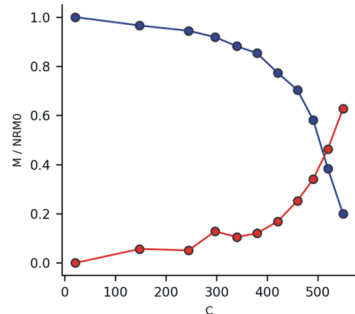
Zijderveld

CM1-12



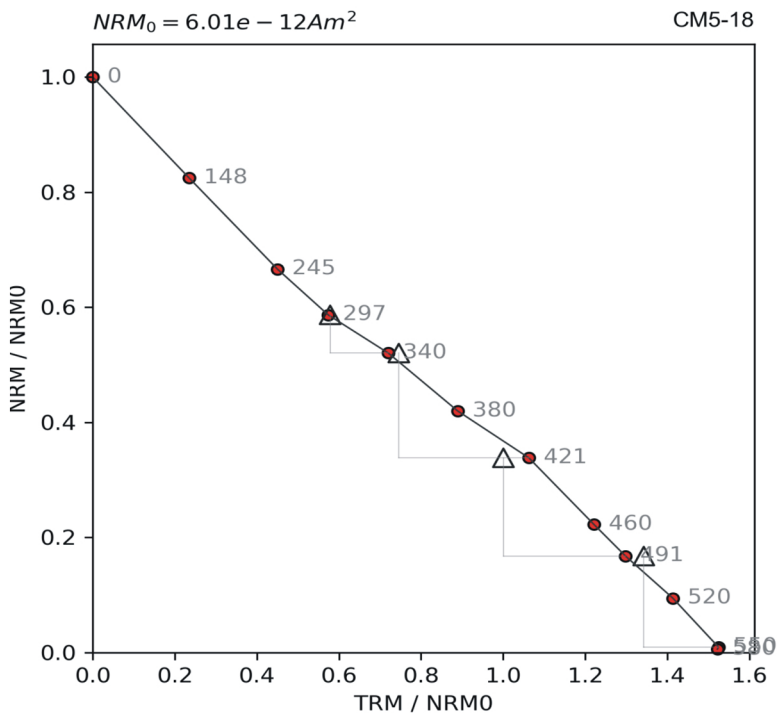
M/T

CM1-12



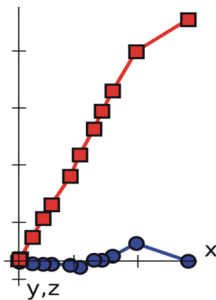
B) Sample CM5-18

Arai plot



Zijderveld

CM5-18



M/T

CM5-18

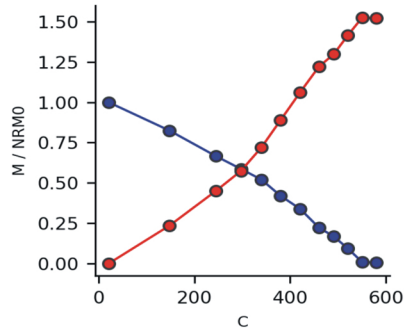
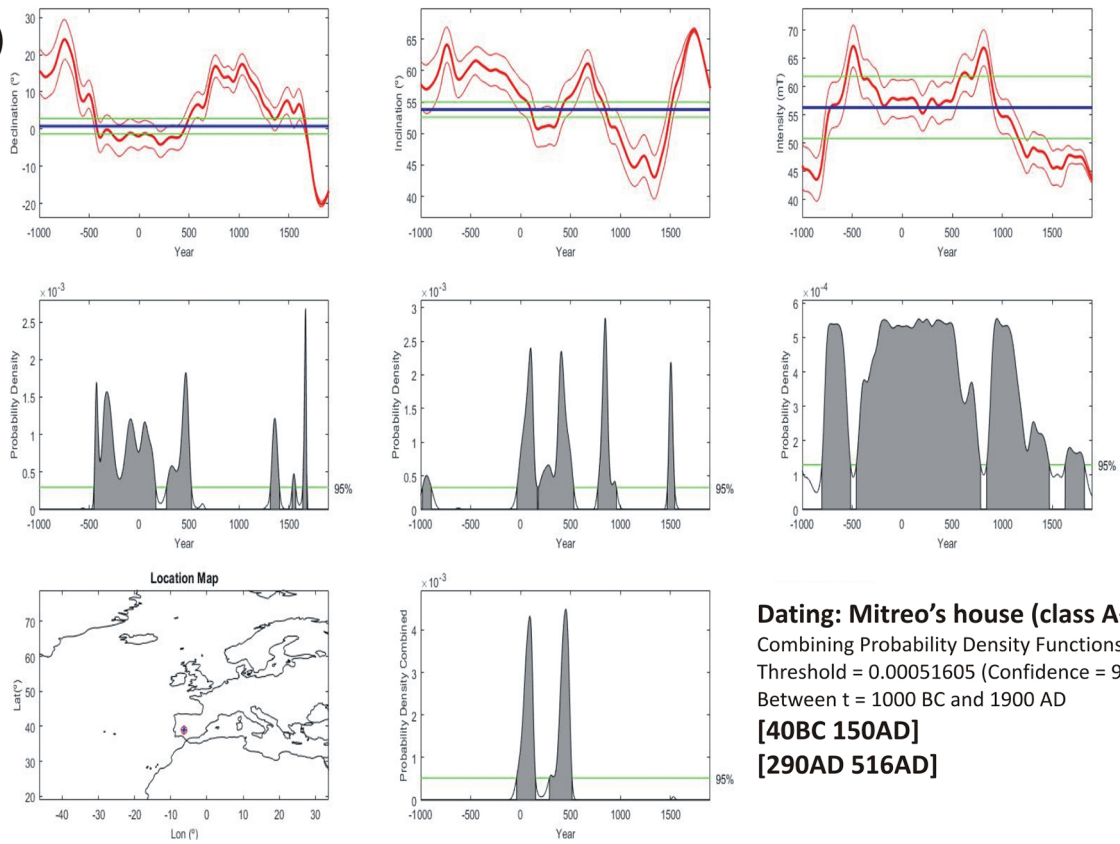


Figure 6

A)



B)

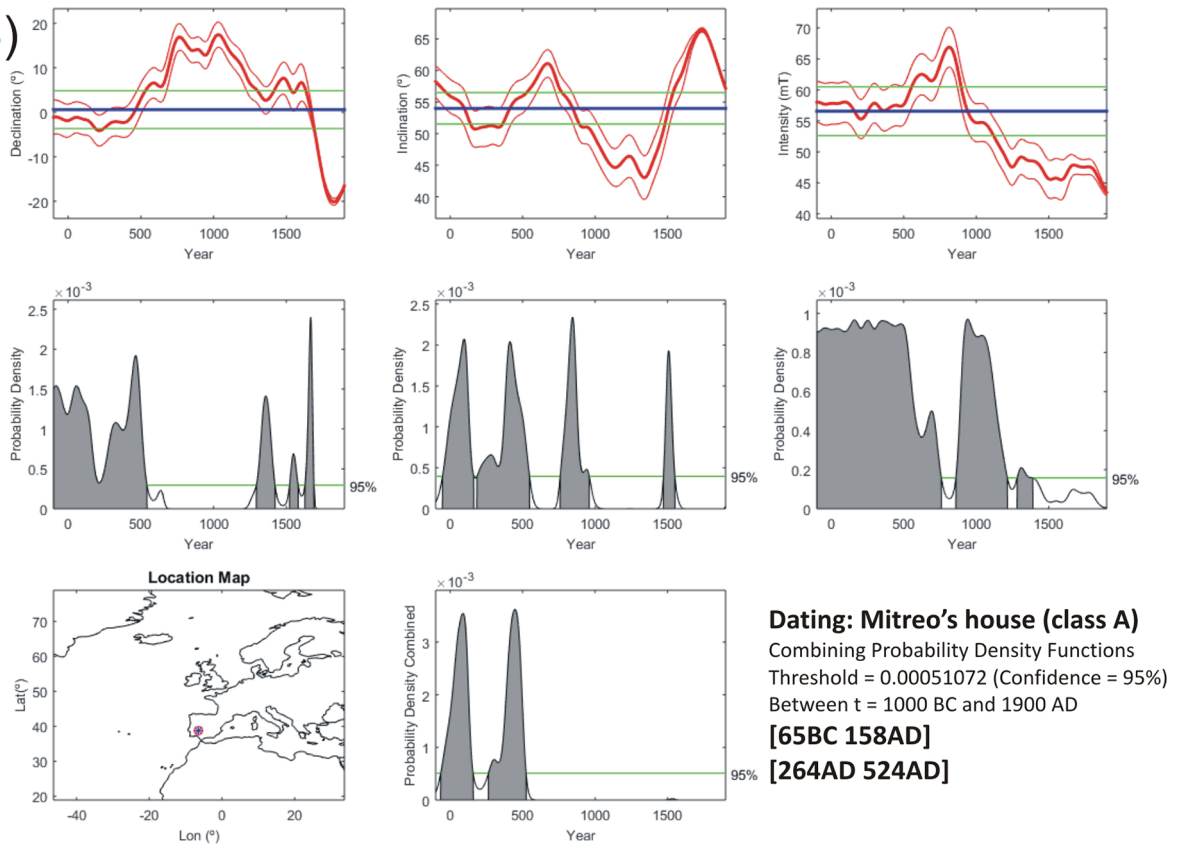
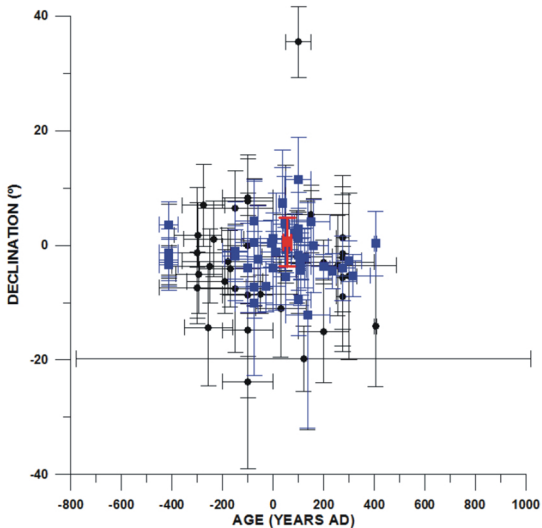
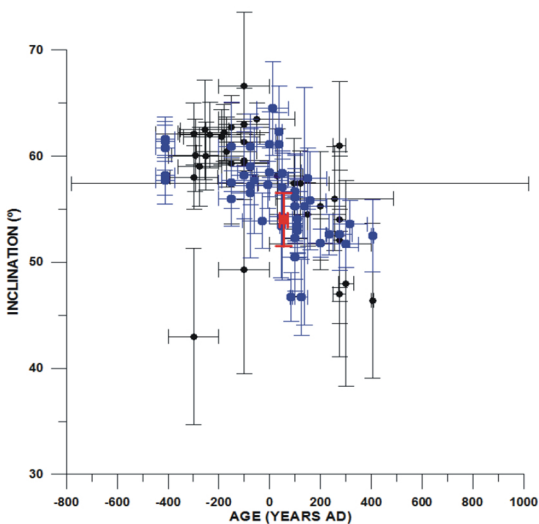


Figure 7

A)



B)



C)

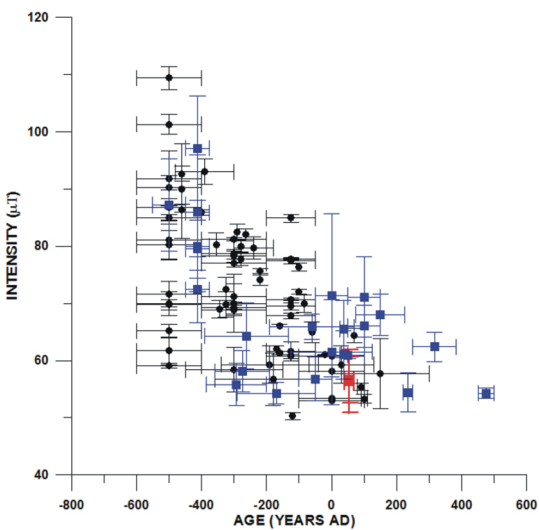


Figure 8